Correlation of Properties and Microstructure in Welded Ti-6Al-6V-2Sn

The use of either a high heat-input welding process or preheat to decrease cooling rates will produce a ductile, tough, stress-corrosion resistant weld with only a small reduction in tensile yield and fatigue strength

BY K. C. WU

ABSTRACT. The purpose of the program described in this paper was to correlate the metallurgical reactions during welding to the mechanical properties and microstructures in a Ti-6Al-6V-2Sn weldment. Welding heat input, material thickness, thermal conductivity, and tooling configuration affect cooling rates in a weldment, and the critical area in titanium-alloy weldments usually is the region where peak temperatures lie between 250°F (1644 K) and the liquidus temperature.

To study the fusion-zone microstructure resulting from various welding processes (cooling rates) and its mechanical properties, four welding processes were used: manual gas tungsten-arc welding (GTAW), plasma arc welding (PAW), automatic gas tungsten-arc welding (GTAW), and electron beam welding (EBW).

Thermal cycles in the heat-affected zone (HAZ) near the fusion line were measured for the four welding processes, and the cooling rates from 2500°F (1644 K) were interpolated or extrapolated. Thus, a correlation between welding processes, cooling rates, and the continuous cooling transformation diagram (CCT) was established, and the relationships between the characteristics of welding processes and the CCT diagrams were identified.

The results obtained from this investigation indicate that:

1. A high heat-input process or the use of preheat to decrease cooling rates will produce a ductile, tough, stress-corrosion resistant weld with a small reduction in tensile yield and fatigue strength.
2. If a low heat-input process is necessary, then postweld heat-treatment at 1400 – 1600°F (1030 – 1140 K) for 4 hours (h) will produce a weld with a tensile yield strength of 147 ksi (1010 MPa) and a minimum fracture toughness of 57 ksi $\sqrt{\text{in.}}$ (1980 MPa $\sqrt{\text{mm}}$).

Introduction

It was found in previous studies (Ref. 1, 2) that the mechanical properties of alpha-beta titanium alloys are cooling-rate sensitive. High cooling rates produce more α and thinner α platelets, which lower toughness and reduce weldability. Slow cooling rates promote the growth of α plates that enrich the β phase with β stabilizers. The enriched phase has a lower Ms temperature and, hence, a lower tendency to transform to α, preferring to remain at room temperature as retained β. Large, tough α plates produced by slow cooling rates divert crack propagation paths and possibly reduce crack propagation by blunting the crack tip. On the other hand, thin martensitic α plates will provide a poorer medium for energy absorption and limit resistance to crack propagation.

Welding processes characteristically deliver various amounts of heat energy in terms of heat-input in Joules per inch (J/in.). Welding processes of low heat-input such as electron beam welding cause high cooling rates that result in low-toughness welds. Welding processes of high-input such as manual gas tungsten-arc welding produce low cooling rates which result in tougher weldments. Other mechanical properties are influenced by cooling rates as well.

The construction of a continuous cooling transformation diagram from a critical peak temperature provides a convenient method for correlating welding processes, heat-input, cooling rate, microstructure, and mechanical properties. Once the effect of cooling rate (welding process) is determined, postweld heat treatments for improving mechanical properties can be explored, if needed, in a systematic manner.

By recording the cooling rates in various welding processes and relating the range of cooling rates for each welding process to the continuous cooling transformation diagram as done in this paper, one may predict the mechanical properties of titanium alloys produced by any welding process.

K. C. WU is Senior Technology Specialist, Metallic Materials Research and Advance Manufacturing Technology, Aircraft Division, Northrop Corporation, Hawthorne, California.

Materials and Procedures

Materials

Four plates of 0.350 in. (8.89 mm) by 36 in. (0.914 m) by 72 in. (1.83 m) Ti-6Al-6V-2Sn and 10 lb (4.54 kg) of 0.040 in. (1.02 mm) diameter Ti-6Al-6V-2Sn filler metal were procured. Both were in the mill-annealed (1350°F or 1010 K – 15 min., air-cooled) condition with chemical analyses within the specification limits.

Specimen Design

Figure 1 shows the specimen geometry for the fusion zone specimens as well as HAZ and base metal specimens. Tensile tests were not used for HAZ specimens due to the size limitation of the synthetic HAZ. The length dimensions of tensile specimens were oriented parallel to the rolling direction of the plate, and fracture toughness and stress-corrosion specimens were machined in the LT orientation.

Construction of Continuous Cooling Transformation Diagram and Simulation of Heat-Affected Zone Specimens

Blanks for mechanical tests and micro-

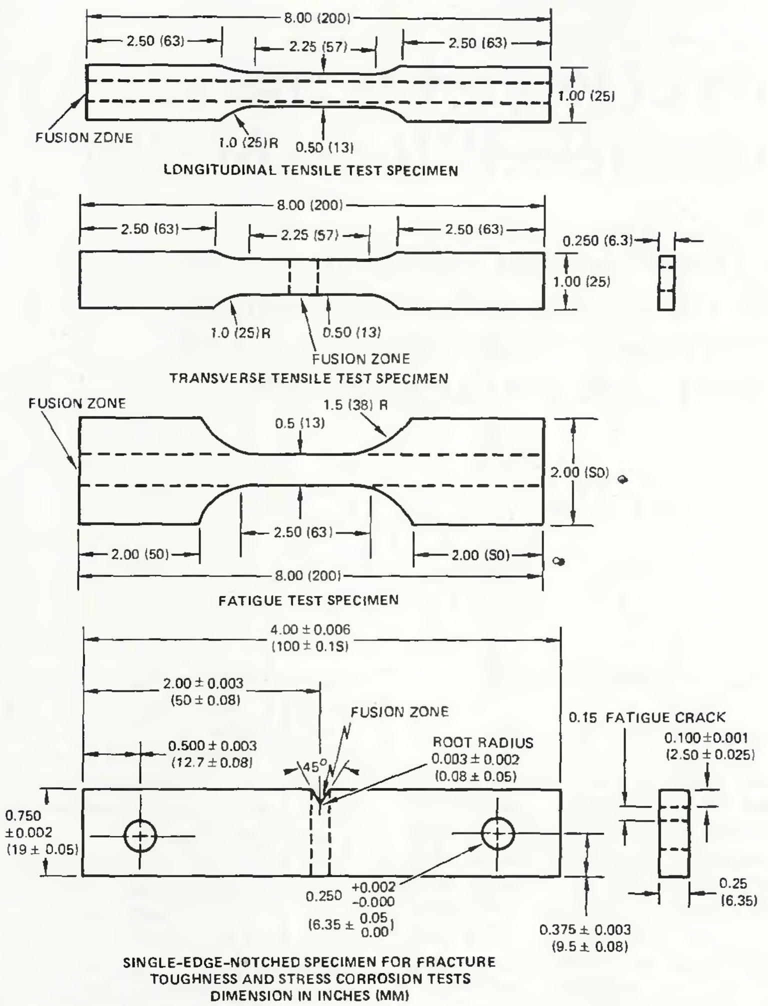

Fig. 1—Configuration of mechanical test specimens

structural analyses were heated to 2500°F (1640 K) in the Gleeble, held at this temperature for 4 seconds (s), and then cooled to room temperature at six different cooling rates: 366°F/s (204 K/s), 280°F/s (156 K/s), 160°F/s (89 K/s), 110°F/s (62 K/s), 64°F/s (36 K/s), and 25°F/s (14 K/s). A high-speed dilatometer and Pt/Pt-10Rh thermocouple were attached to each specimen for recording specimen dilation and thermal cycle on an oscillograph.

Specimens in each cooling-rate group were divided into three subgroups of three each. Each subgroup was tested in a different condition:

1. As-cycled.
2. Cycled plus 1400°F (1033 K) for 4 h.
3. Cycled plus 1600°F (1144 K) for 2 h.

Welding

Four welding processes were used: manual GTA, plasma arc, automatic GTA, and electron beam welding—Table 1. The double-V joint configuration was used for manual and automatic GTA welding, and square butt joints were used for electron beam and plasma arc welding.

Postweld Heat treatment

Either simulated HAZ blanks or weldments were machined to their final dimensions before heat-treatment. Two heat-treatments—1400°F (1033 K) for 4 h and 1600°F (1144 K) for 2 h, followed by air cooling, were selected for HAZ zone specimens. Since a 1200°F (922 K) heat treatment did not improve HAZ toughness (Ref. 3), heat-treatment temperatures higher than this were required. A treatment of 1400°F (1033 K) for 4 h is simple and can be conducted in air without serious oxidation. However, in this program, all heat-treatments were conducted in a vacuum furnace operating at approximately 10^{-5} torr (1.33×10^{-3} Pa). Fusion zone specimens were heated to 1400°F (1033 K) for 4 h.

Microstructural Studies

Microstructural studies conducted in this program included optical photomicrography and x-ray diffraction. The standard metallographic method was used to prepare specimens for microstructural and macrostructural studies. X-ray diffraction techniques were applied to study phase transformations.

Mechanical Testing

Hardness Measurements. Rockwell C-scale was used for hardness measurements to meet industrial practices. When the microstructure varied in a small region, Knoop microhardness measurements were used and Knoop hardness numbers were converted to Rockwell C numbers. Five measurements were made on each specimen to obtain an average hardness value.

Tensile Tests. A grid was printed on the reduced section of each tensile specimen to register the local elongation in the weld. However, no significant variation in local elongation or lateral contraction was observed.

Fracture-Toughness and Stress-Corrosion Tests. The precracked single-edge-

Table 1—Welding Schedules for Automatic GTA, Manual GTA, Plasma Arc, and Electron Beam Welding

Process	Travel, ipm. (m/min)	Arc voltage V	Welding current A	Torch cfh. (L/min)	Shielding gas, cfh. (L/min)	Trailing gas, cfh. (L/min)	Backing gas, cfh. (L/min)	Fiber metal feed, ipm. (M/min)
Manual GTA	2 approx. (0.05)	8-11	Vary[a]	–	–	–	–	Manual
Plasma arc	6 (0.30)	30	180[a]	30 (14.2)	4 (1.89)	60 (28.3)	20 (9.44)	None
Electron beam	40 (1.02)	130×10^{-3}	35×10^{-3}	–	–	–	–	None
Automatic GTA	6 (0.30)	9 – 10	260-270[a]	20 (9.44)	–	50 (32.6)	15 (7.08)	42 (0.018)

[a]DC straight polarity.

Table 2—Tensile, Fracture Toughness, and Stress-Corrosion Behavior of Ti-6Al-6V-2Sn Plate in MA and STA Conditions

	Yield strength, ksi (MPa)	Ultimate strength, ksi (MPa)	Elongation, % in 2 in. or 50 mm	K_{Ic}, ksi $\sqrt{inch}$ (MPa $\sqrt{mm}$)	K_{Iscc}, ksi $\sqrt{inch}$ (MPa $\sqrt{mm}$)
MA	152.7 (1,052)	161.2 (1,111)	13.0	44 (1,530)	35 (1,216)
STA	186.3 (1,284)	195.9 (1,350)	5.0	24 (834)	21 (730)

notch specimen shown in Fig. 1 was used to determine the stress-corrosion behavior and fracture toughness of the base metal, simulated heat-affected zone, and fusion zone. This specimen configuration closely resembles design recommendations by Srawley and Brown (Ref. 4) and Payne (Ref. 5) for plane-strain fracture toughness tests. The synthetic HAZ specimens were thermally cycled before notching in order to maintain a constant cross-section for uniform resistance heating in the Gleeble.

Each stress-corrosion specimen was precracked on the same machine and with the same basic procedure as the fracture-toughness test specimens, with one exception. The notch was submerged in 3.5% salt water in a plastic box attached to the specimens during precracking and until the completion of the stress-corrosion test. The specimen was loaded using a dead-weight level-arm frame. Weight equivalent to 1.0 ksi $\sqrt{in.}$ (34.7 MPa $\sqrt{mm}$) was added every 3 h, minimum, until crack growth initiated and/or the specimen failed.

Results and Discussion

Characterization of Base Metal

To provide a baseline for comparison, the mechanical and metallurgical properties of the base metal were determined. The base metal in the mill annealed condition and solution-treated and aged (STA) condition (1650°F or 1170 K – 1 h, WQ and 1050°F or 839 K – 4 h, air-cooled) was characterized by tension, fracture toughness, and stress-corrosion tests – (Table 2).

Microstructures of the base metal in the MA (mill annealed) and STA conditions (solution treated and aged) are shown in Figs. 2 and 3. X-ray diffraction measurements indicated that the base metal contained 93% α and 7% β in the MA condition and 86% α, 8% α' and 6% β in the STA condition.

Heat-Affected Zone Studies

Continuous Cooling Transformation. Figure 4 shows the continuous cooling transformation diagram (CCT) determined for Ti-662 from 2500°F (1640 K), based upon six cooling rates. Mechanical properties were determined and microstructure studies were conducted on specimens cooled at 366°F/s (203 K/s), 110°F/s (61 K/s). and 25°F/s (14 K/s).

The $\beta \rightarrow \alpha$ transformation temperature decreased with increasing cooling rate (1500°F at 25°F/s or 1090 K at 14 K/s and 1230°F at 366°F/s or 939 K at 203 K/s). It was expected that the nucleation and growth process would be suppressed by increasing the cooling rate. For the same reason, the α platelets were narrower and shorter at higher cooling rates, as shown in the microstructures of Fig. 5. The CCT diagram further shows that the martensitic transformation temperature (Ms) has not been affected by cooling rate, as found in Ti-Mo alloys by Duwez (Ref. 6), because the transformation of $\beta \rightarrow \alpha'$ is a shear process. The Ms temperature is approximately 1040°F (833 K).

On cooling, the β phase became unstable at the α/β transformation temperature, and α phase precipitated by rejecting β stabilizers. At the Ms temperature, lean β phase transformed to α' by shear, and enriched β phase, which has a lower Ms temperature, remained as retained β.

At slow cooling rates, the time for nucleation and growth of α phase is longer and the size of α-platelets is larger. Furthermore, β stabilizers diffuse from the growing of phases into the surrounding β phases. This enrichment of β stabilizers increases the amount of stable β phase. Therefore, less unstabilized β phase is available to transform into α'. When the cooling rate is high, there is less time for nucleation and growth of α phase, and the size of α platelets is small. Since less α phase transforms from β, the β phase is more diluted in β stabilizers. Thus, more α' is transformed below the Ms temperature.

Effect of Cooling Rate on Microstructure and Mechanical Properties. Figure 6 indicates the effect of cooling rate on phase contents in the synthetic HAZ. In the as-cycled condition, the phases present were 60% α, 30% α', and 10% β in a specimen cooled from 2500°F at 366°F/s (1644 K at 203 K/s). At 25°F/s (14 K/s), the α phase increased to 81% and α' phase decreased to 10%. However, cooling rate was less influential on the β

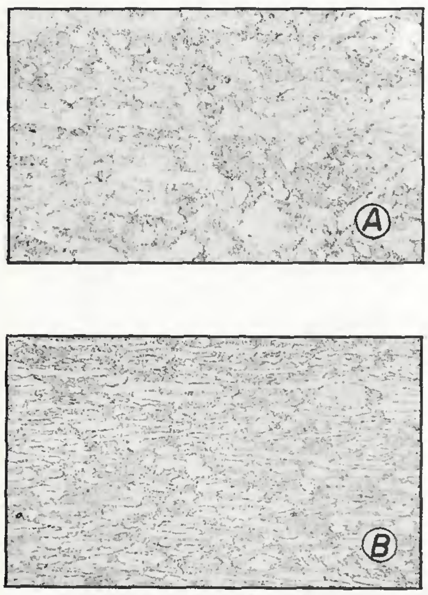

Fig. 2 – As-received base metal (mill annealed) microstructure: A – top view; B – transverse view, R_c 35 hardness. X500 (reduced 50% on reproduction)

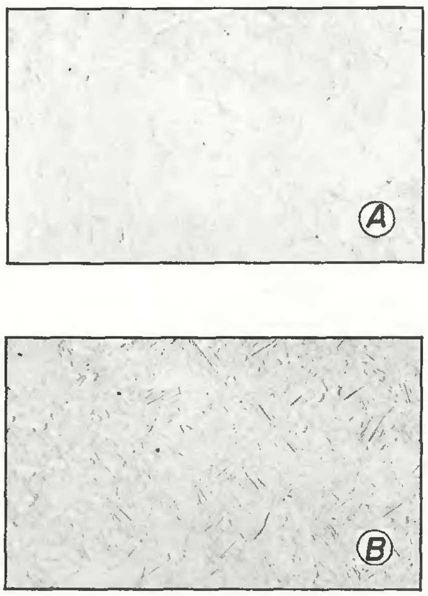

Fig. 3 – Microstructure of base metal solution treated as follows: 1650°F (1170 K) – 1 h water quench – aged 4 h at 1050°F (839 K). A – top view; B – transverse view, R_c 41 hardness. X500 (reduced 50% on reproduction)

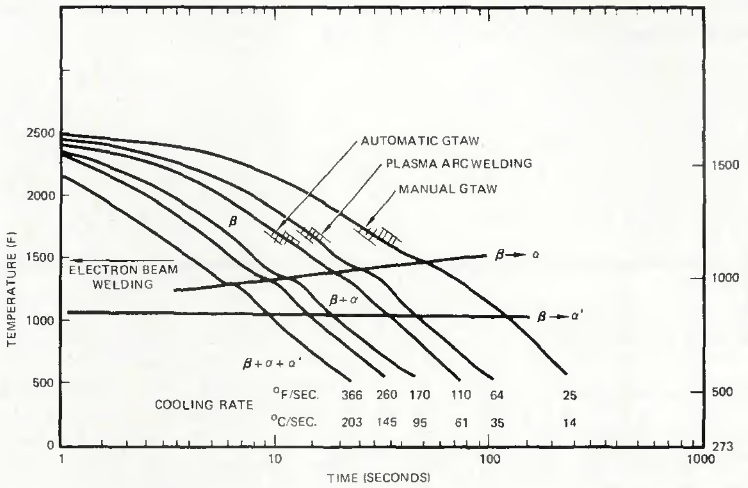

Fig. 4 — Continuous cooling transformation diagram for Ti-6Al-6V-2Sn

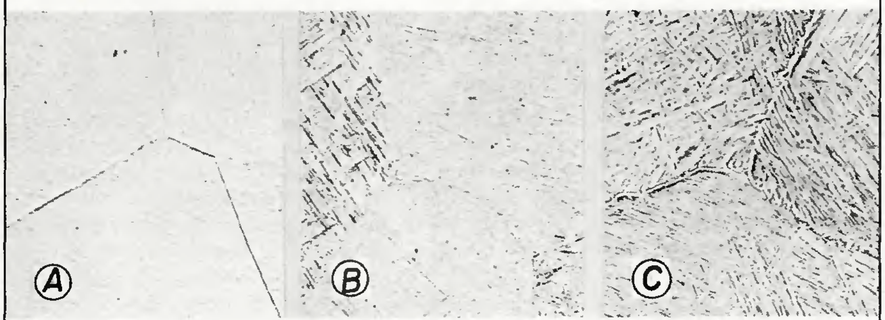

Fig. 5 — Synthetic HAZ microstructure cooled as follows: A — at 366°F/s (203 K/s); B — at 110°F/s (61 K/s); C — at 25°F/s (14 K/s). X500 (reduced 47% on reproduction)

content, which remained between 5% and 10%.

Microstructure has a definite influence on the mechanical properties. Hardness measurements were the least sensitive measure of microstructural changes — (Table 3). Yet, they show the general trend of higher hardnesses at high cooling rates.

Figures 7 and 8 show the effect of cooling rate on fracture toughness and stress-corrosion resistance in three conditions. Considering the as-cycled condition only, Fig. 8 indicates that the cooling rate had a large influence on the fracture toughness. Increasing the cooling rate from 25°F/s (14 K/s) to 366°F/s (203 K/s) decreased K_{Ic} from 60 ksi $\sqrt{in.}$ (2080 MPa $\sqrt{mm}$) to 34 ksi $\sqrt{in.}$ (1180 MPa $\sqrt{mm}$). The stress-corrosion resistance (Fig. 8) only decreased from 38 ksi $\sqrt{in.}$ (1320 MPa $\sqrt{mm}$) to 32 ksi $\sqrt{in.}$ (1100 MPa $\sqrt{mm}$) due to the same change in cooling rates.

From the CCT diagram, one can predict that the transformation products resulting from various cooling rates affect the mechanical properties. Figure 9 shows that K_{Ic} is decreased with increasing amounts of α' and decreasing amounts of α, but is not related to the amount of β. The decreased fracture toughness from increasing volume fractions of metastable phases (α' in this case) was discussed by Curtis and Spurr (Ref. 7).

The morphology of α-platelets also affects toughness. Thinner α-platelets produced by higher cooling rates decrease toughness. It is believed that the combined effects of increasing α' and decreasing α-platelet size are responsible for the decreased toughness in a weldment. Both the amount of α' and the α-platelet size are uniquely related to cooling rate. Figure 10 is a plot of the effect of phase contents on K_{Iscc}. A comparison of Figs. 9 and 10 shows that K_{Ic} was decreased substantially more than K_{Iscc} with increasing amounts of α

Fracture toughness of the HAZ's varied considerably, depending upon welding parameters and post weld treatments. Therefore, stress-corrosion behavior was also examined in terms of the ratio of K_{Iscc}/K_{Ic} to normalize differences in toughness. The effects of cooling rates and phase contents on the stress-corrosion susceptibility ratio (K_{Iscc}/K_{Ic}) are plotted in Figs. 11 and 12, respectively.

It is important to realize that an increase in the K_{Iscc}/K_{Ic} ratio reflects a decrease in the stress-corrosion susceptibility of a material. In the as-cycled condition, then, increasing cooling rates decreased stress-corrosion susceptibility appreciably — Fig. 11. However, stress-corrosion susceptibility was less dependent upon cooling rate when a post weld heat treatment was employed.

Figure 12 shows a strong trend of decreasing stress-corrosion susceptibility (increasing K_{Iscc}/K_{Ic} ratio) with increasing amounts of α'. At approximately 30% α', K_{Iscc}/K_{Ic} was essentially equal to one, indicating immunity to stress-corrosion. However, it must be appreciated that K_{Ic} and K_{Iscc} decreased with increasing amounts of α', even though the ratio of K_{Iscc}/K_{Ic} increased. The stress-corrosion immunity of microstructures containing substantial amounts of α' has also been

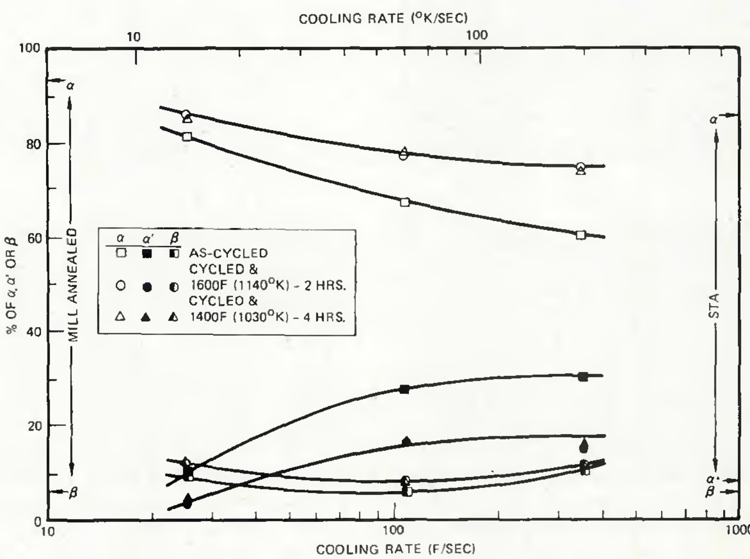

Fig. 6 — Effect of cooling rate on phase contents in the synthetic HAZ before and after heat treatment at 1600°F (1140K) — 2 h

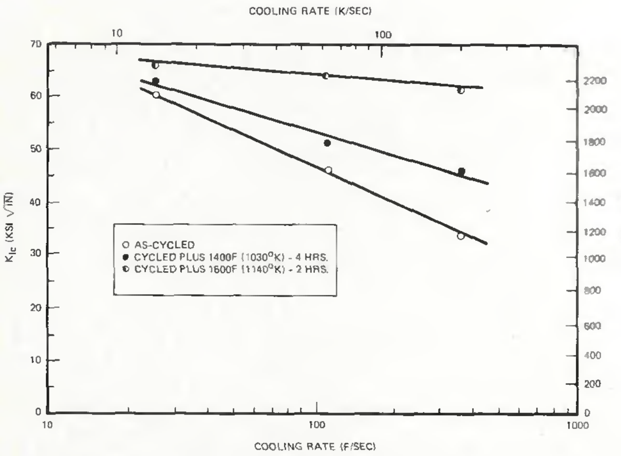

Fig. 7—Effect of cooling rate and post-cycle heat treatment on fracture toughness of the synthetic HAZ

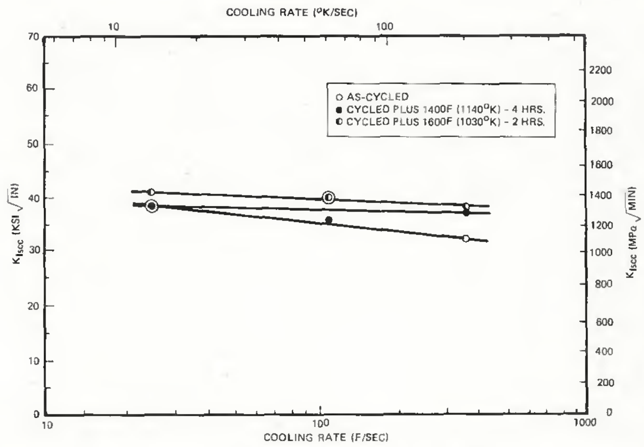

Fig. 8—Effect of cooling rate and post-cycle that treatment on stress-corrosion resistance of the synthetic HAZ

Table 3—Synthetic HAZ Hardness, Rockwell C

Rate, °F (K)/s	As-cycled	Cycled plus . . . 1400°F (1030 K) −4h	1600°F (1140 K) −2 h
366 (203)	45	37	33
260 (144)	42	—	—
170 (94)	39	—	—
110 (61)	41	36	35
64 (36)	39	—	—
25 (14)	36	34	34

noted in Ti-6Al-4V and Ti-8Al-1Mo-1V alloys by Fager and Spurr (Ref. 8).

Effect of Heat Treatment on Synthetic HAZ Microstructure and Mechanical Properties. Welding processes that produce a high heat input also produce a HAZ of high toughness and stress-corrosion resistance. From a metallurgical point-of-view, such welding processes are ideal for joining Ti-6Al-6V-2Sn. Unfortunately, high heat-input processes produce narrow and deep fusion zones that are preferred for aircraft application because of fit-up, joint design, distortion, and economic considerations. In these cases, low toughness and stress-corrosion resistance are expected in the HAZ. To improve the mechanical properties, postweld heat treatment must be performed. In this investigation, two heat-treatment conditions were employed: 1400°F (1033 K) for 4 h and 1600°F (1144 K) for 2 h, followed by air cooling in both cases.

Figure 13 shows the microstructure of specimens that experienced cooling rates from 2500°F (1640 K) of 366, 100, and 25°F/s (203, 56, and 14 K/s), followed by heat treatment at 1400°F (1030 K) for 4 h. This heat treatment coarsened α-platelets and promoted some decomposition of α' to $\alpha + \beta$. A heat treatment of 1600°F (1140 K) for 2 h promoted further coarsening of α platelets and decomposition of α' to $\alpha + \beta$—Fig. 14.

As a result of the changes in phase contents by heat treatments, the K_{Ic} and K_{Iscc} values were affected. In Fig. 7, heat treatment not only increased the fracture toughness but also reduced the differences in fracture toughness caused by differences in cooling rates.

The effect of heat treatment on the stress-corrosion susceptibility was shown in Fig. 11. Heat treatment increased stress-corrosion susceptibility (lower K_{Iscc}/K_{Ic} ratio) by greater amounts for high cooling rates than for low cooling rates. The heat treatment at 1600°F (1144 K) for 2 h increased the stress-corrosion susceptibility more than heat treatment at 1400°F (1033 K) for 4 h, and also eliminated the cooling rate effect.

The effect of heat treatment on the stress-corrosion susceptibility is again attributed to the phase transformation products and microstructural morphology. If one compares Figs. 6 and 11, the curves in Fig. 6 are similar but inverted from Fig. 11. Figure 12 includes data points obtained from all conditions. It is

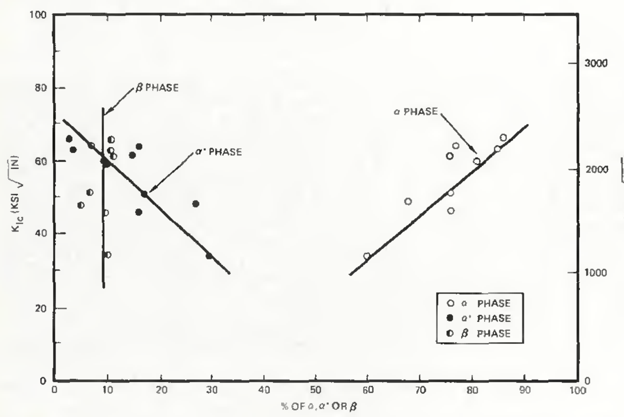

Fig. 9—Effect of phase contents on fracture toughness of the synthetic HAZ, as-welded and heat-treated conditions

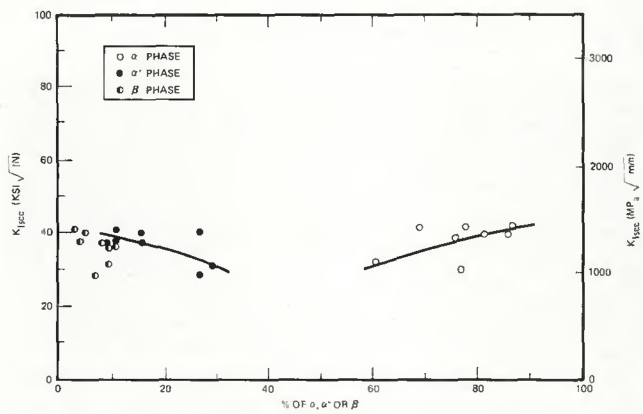

Fig. 10—Effect of phase contents on stress-corrosion resistance of the synthetic HAZ, as-cycled and heat-treated conditions

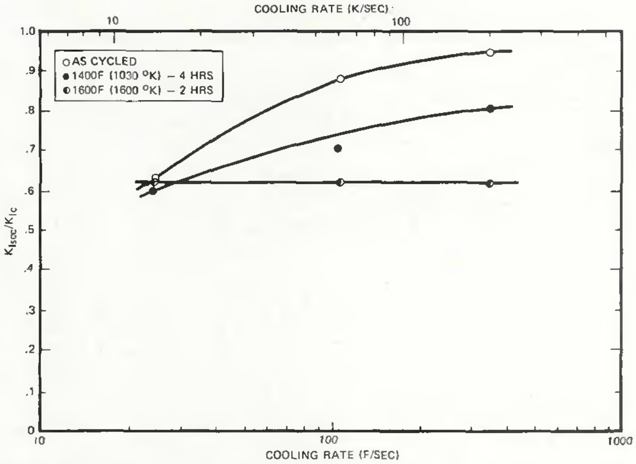

Fig. 11—Effect of cooling rate on stress-corrosion susceptibility of the synthetic HAZ

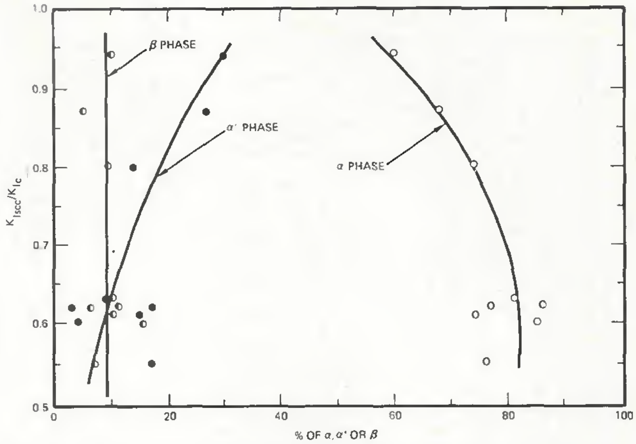

Fig. 12—Effect of phase contents on stress-corrosion susceptibility of the synthetic HAZ, as-welded and heat-treated conditions.

clearly shown that the stress-corrosion susceptibility is related to the microstructural morphology, particularly α' and, probably, fine α precipitates.

Fusion Zone Studies

Correlation Between Heat Input and Cooling Rate. One of the important parameters of welding processes is the heat input in terms of Joules per inch (J/in.). Therefore, the selection of the welding processes should consider not only the economics and practicality of the process, but also the metallurgical effects related to the different heat inputs of the welding processes. The heat inputs and cooling rates for the four welding processes are listed in Table 4.

The corresponding cooling rate for each process on the CCT diagram is shown in Fig. 4. The hatched lines indicate the probable variations in cooling rates caused by typical variations of welding parameters, material thickness, and backing material. It should be noted that the microstructure and mechanical properties in the fusion zone may not be the same as that of the HAZ near the fusion line because of melting and solidification during welding.

Effect of Processes on Microstructure and Mechanical Properties of the Fusion Zones. Figure 15 shows the microstructures in the fusion zones produced by the four welding processes. It is obvious that the fineness of the α-platelets is related to the cooling rate associated with each welding process. More feather-like α is observed in the manual GTA weld, Fig. 15A, than in welds produced by the other welding process. On the other hand, the needles in the electron-beam fusion zone are so fine that they are hardly resolved—Fig. 15D. The needle size in Figs. 15B and 15C is between these two extremes.

From the CCT diagram (Fig. 4), once again we can predict that the fusion zones contain different amounts of phases due to differences in cooling rates. The results from x-ray diffraction measurements of the α, α', and β contents are shown in Fig. 16. As expected, the phase contents are entirely related to the cooling rate. The cooling rate in the HAZ of the electron beam welds was greater than 1000°F/s (556 K/s); therefore, dotted lines are used.

The room-temperature tensile test data are shown in Table 5. The longitudinal tensile specimens exhibited strengths which averaged the strengths of the base metal, HAZ, and fusion zone (FZ). The tensile strengths, as well as yield strengths obtained from the longitudinal specimens, are about the same within a variation of 1.5%. Elongation data show a weak trend of lower elongation with increasing cooling rate, except for the electron beam welds. This was due to the fact that the gage section of the EB-welded tensile specimens contained more base metal than the specimens produced with the other welding processes.

In the transverse tensile tests, failure took place in the weakest zone. With the exception of manual GTAW, failure occurred in the base metal instead of the fusion zone. This occurred because the α' and fine α platelets produced at higher cooling rates strengthened the fusion zones and part of the heat-affected zones. Although the manual GTAW produced more α' in the fusion zone than in the base metal, failure took place in the fusion zone because of the extremely large columnar structure. Because failure took place in the base metal in the welds produced by the other three welding processes, the tensile yield strengths were essentially identical as shown in Table 5. However, the elongation in the electron beam welds was extremely high (13.5%) in comparison to the other welds (8–9.7%). This was apparently caused

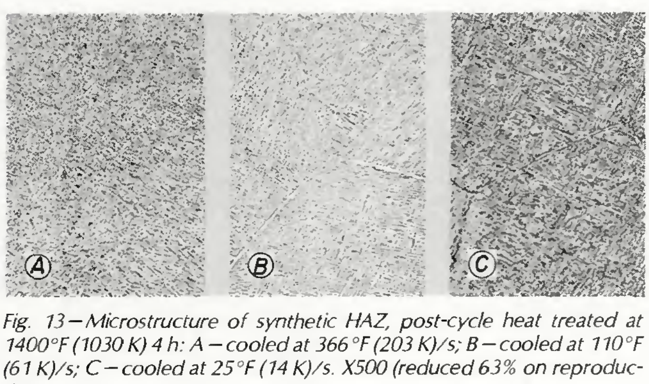

Fig. 13—Microstructure of synthetic HAZ, post-cycle heat treated at 1400°F (1030 K) 4 h: A—cooled at 366°F (203 K)/s; B—cooled at 110°F (61 K)/s; C—cooled at 25°F (14 K)/s. X500 (reduced 63% on reproduction)

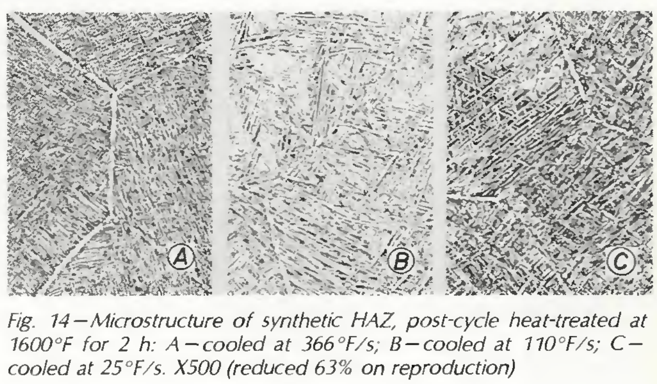

Fig. 14—Microstructure of synthetic HAZ, post-cycle heat-treated at 1600°F for 2 h: A—cooled at 366°F/s; B—cooled at 110°F/s; C—cooled at 25°F/s. X500 (reduced 63% on reproduction)

Table 4—Heat Inputs and Cooling Rates for Four Welding Processes

	Heat input, kJ/in. (kJ/m)	Cooling rate, °F/s (K/s)
Manual GTAW[a]	78 (3070)	25 (14)
Plasma arc	54 (2130)	64 (36)
Automatic GTAW[a]	26 (1020)	110 (61)
Electron beam	7 (276)	1000 (556)

[a]Welded from both sides.

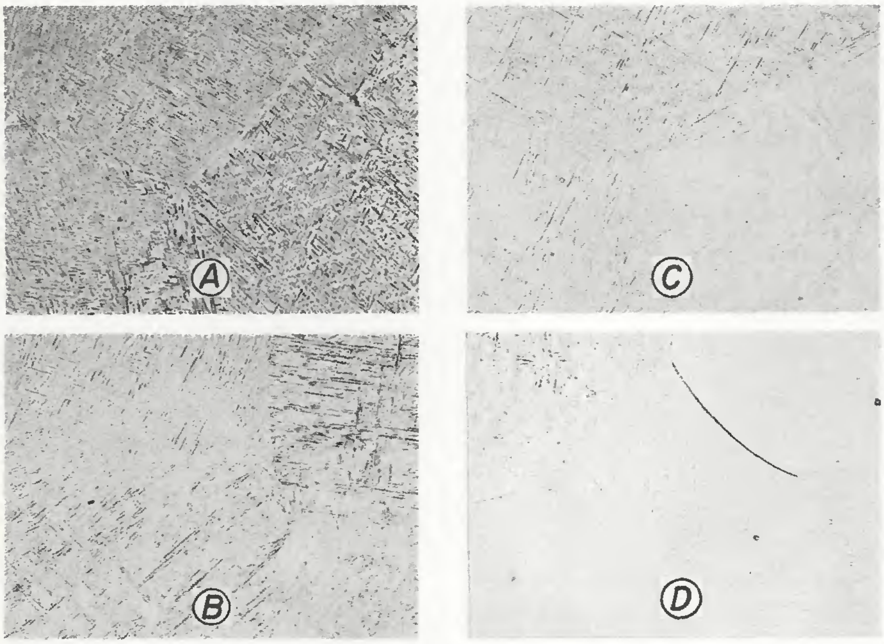

Fig. 15—As-welded microstructure of fusion zones welded with four processes: A—manual GTAW; B—plasma arc; C—automatic GTAW; D—electron beam. X500 (reduced 46% on reproduction)

by the ratio of the fusion zone width to the base metal width within the gage length that was the smallest for the electron beam weld.

Fracture and stress-corrosion susceptibility were affected by α' content as observed in HAZ studies and therefore, were a function of cooling rate, which was a characteristic of welding processes as shown in Fig. 17.

Effect of Postweld Heat Treatment on Fusion-Zone Microstructure and Mechanical Properties. The postweld heat treatment used for the fusion-zone tests was 1400°F (1033 K) for 4 h in a vacuum furnace. This heat treatment was also one of those used for the synthetic HAZ tests. Higher temperatures will produce a microstructure which provides better toughness and ductility based upon the HAZ studies.

The microstructure of the fusion zone at X500 is shown in Fig. 18. The α-platelets in the grains grew larger, and continuous α precipitates appear in the grain boundaries (compare to Fig. 15C). The microstructure here is identical with the microstructure in the HAZ cooled at 110°F/s (61 K/s) and heat treated at 1400°F (1033 K) for 4 h—Fig. 13B.

When α was growing during this heat treatment, the transformation of α' to $\alpha + \beta$ was taking place. As a result of this transformation, α content after heat treatment was increased from 75 to 86%, β content from 9 to 11%, and α' content was reduced from 16 to 3%. Because of the change of microstructure, morphology, and phase contents, the mechanical properties were affected accordingly.

A postweld heat treatment of 1400°F (1033 K) for 4 h was expected to reduce tensile and yield strengths and increase elongation in the fusion zone. Table 6 lists the tensile test results. Comparison with

Table 5—Tensile Properties of Welded Ti-6Al-6V-2Sn Plate As-Welded

Process[a]		Yield strength, ksi (MPa)	Ultimate tensile strength ksi (MPa)	Elongation in 2 in. (or 50 mm) %	Modulus, 10^6 psi (GPa)	Failure location[a]
Manual GTAW	L	153.3 (1056)	171.8 (1184)	4.0	15.3 (105)	—
	T	154.6 (1065)	167.5 (1154)	4.7	16.3 (112)	FZ
PAW	L	155.7 (1073)	173.2 (1193)	3.7	15.0 (103)	—
	T	162.3 (1118)	175.8 (1211)	9.7	16.2 (112)	BM
Automatic	L	157.6 (1086)	175.2 (1207)	3.5	15.3 (105)	—
	T	163.8 (1129)	174.8 (1204)	8.0	17.0 (117)	BM
EBW	L	155.9 (1074)	172.6 (1189)	5.2	15.1 (104	—
	T	163.3 (1125)	173.0 (1191)	13.5	17.3 (119)	BM

[a]L—longitudinal tension; T—transverse tension; BM—base metal; FZ—fusion zone.

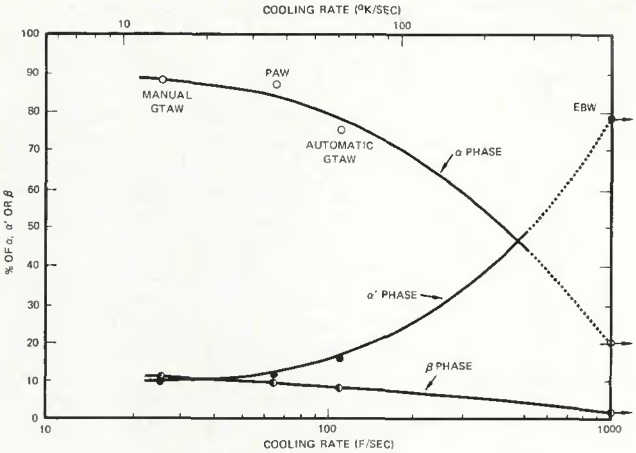

Fig. 16—Effect of cooling rate on phase contents in as-welded fusion zones

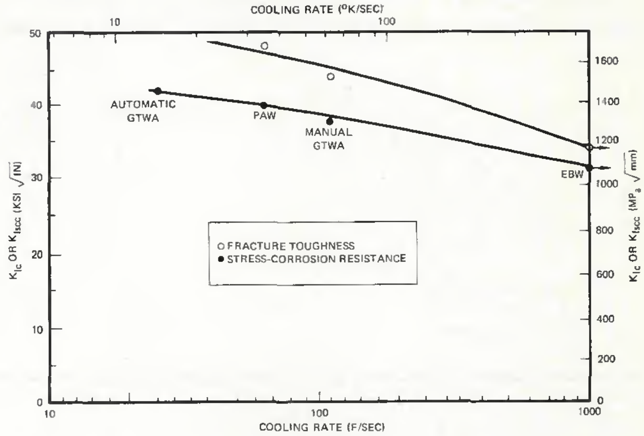

Fig. 17—Effect of cooling rate on fracture toughness and stress-corrosion resistance of as-welded fusion zones.

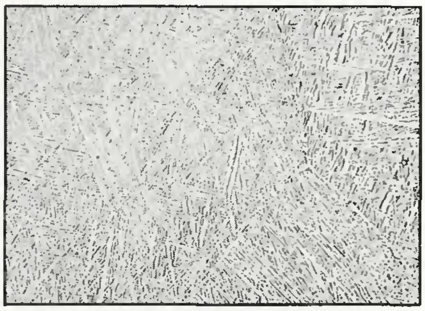

Fig. 18—Microstructure of automatic GTA welded fusion using Ti-622 filler metal, 1400°F (1030 K) — 2 h. X500 (reduced 50% on reproduction)

the as-welded, longitudinal tensile properties (Table 5) produced by automatic GTAW demonstrates this effect.

The transverse tensile tests showed the failure location to be in the fusion zone instead of in the base metal as in the as-welded condition. The narrow fusion zone (about 0.5 in. or 12.7 mm), compared to the 2 in. (50 mm) gage length, limited the elongation to 9%.

The postweld heat treatment reduced the amount of α' in the fusion zone and this reduction increased fracture toughness from 44 ksi $\sqrt{in.}$ (1530 MPa $\sqrt{mm}$) in the as-welded condition to 57 ksi $\sqrt{in.}$ (1980 MPa $\sqrt{mm}$). However, the stress-corrosion resistance remained about the same (36 ksi $\sqrt{in.}$ or 1250 MPa $\sqrt{mm}$) as observed for the as-welded condition (37 ksi $\sqrt{in.}$ or 1285 MPa $\sqrt{mm}$).

The FZ studies show that the effects of postweld heat treatment on fracture toughness and stress-corrosion resistance were similar to the effects observed in the HAZ studies.

Table 6—Tensile Properties of the Fusion Zone, Automatic GTAW Postweld Heat-Treated at 1400°F for Four Hours—Average of Three Tests.

	Longitudinal tension	Transverse tension
Yield strength, ksi	147.4	155.6
(MPa)	(1016)	(1072)
Ultimate tensile strength, ksi	158.9	164.8
(MPA)	(1095)	(1135)
Elongation in 2 in. (or 50 mm), %	11.8	9.0
Modulus, 10^6 psi	16.4	17.5
(GPa)	(113)	(121)
Failure location	—	FZ[a]

[a]FZ—fusion zone.

Conclusions

Based upon the experimental results, conclusions can be drawn as follows:

1. Correlation has been established between the heat input of welding processes and cooling rates of heat-affected zones.
2. A continuous cooling transformation diagram can be used to predict the mechanical properties in the fusion and heat-affected zones produced by various welding processes.
3. Fracture toughness in the weld can be improved by slow cooling or postweld heat treatment at or above 1400°F (1033 K).
4. Alpha-prime and thin α-platelets reduce fracture toughness but improve resistance to stress-corrosion.
5. The results of this investigation showed how Ti-6Al-6V-2Sn can be welded to achieve a fracture toughness of 57 ksi $\sqrt{in.}$ (1980 MPa $\sqrt{mm}$) minimum with a yield strength of 147 ksi (1013 MPa).

Acknowledgment

This paper is based on the program entitled "Correlation of Properties and Microstructure in Welded Titanium Alloys," AFML-TR-73-202 Contract No. F33615-72-C2015, sponsored by the Air Force Materials Laboratory, Wright-Patterson Air Force Base, Ohio. The author wishes to thank Captain R. P. Simpson, AFML, the Project Engineer, and Mr. A. H. Freedman, Materials Research Department, Northrop Corporation, Aircraft Division, for their guidance and valuable discussions in the course of this program. Technical assistance contributed by Messrs. R. E. Herfert, G. A. Blake, J. W. Lewis, H. E. Langman, and L. Goltra in various areas is deeply appreciated.

References

1. Wu, K. C. 1965. Weldability study of titanium 8Al-1Mo-1V, Rene 41, and Rene 63. Northrop report NOR 65-250, October.
2. Wu, K. C. 1961. Qualitative evaluation of the heat-affected zone in the tungsten inert gas welding of titanium alloys. Watervliet Arsenal memorandum report, May 19.
3. Lewis, R. E., and Wu, K. C. 1963. A study of weld heat-affected zone in titanium 6Al-6V-2Sn. *Welding Journal* 42 (6): 241-s to 251-s.
4. Srawley, J. E., and Brown, W. F. 1965. Fracture toughness testing. NASA TN-D-2599, January.
5. Payne, W. W. 1965. Practical specimens for K_{IC} measurement. Second annual workshop in fracture mechanics, August. Denver University.
6. Duwez, P. 1951. Effect of cooling on the alpha-beta transformation in titanium and titanium-molybdenum alloy. *Journal of Metals*, September: 765.
7. Curtis, R. E., and Spurr, W. F. 1968. Effect of microstructure on the fracture properties of titanium alloys in air and salt solution. *Transactions ASM* 61 (3): 115.
8. Fager, D. F., and Spurr, W. F. 1968. Some characteristics of aqueous stress-corrosion in titanium alloys. *Transactions ASM* 61 (6): 283-292.